A Novel UHF-RFID Dual Antenna Signals Combined with Gaussian Process and Particle Filter for In-pipe Robot Localization

Amal Gunatilake, Sarath Kodagoda, and Karthick Thiyagarajan

***Abstract*— Condition assessment of underground infrastructures such as pipe networks is crucial for aging cities around the globe. Recent development of robotic technologies facilitated application of them in condition assessment of pipe networks. However, there is still a gap for accurate localization technology in pipes due to complexity of the environment. In this letter, we propose a novel ultra-high frequency radio frequency identification (UHF-RFID) technology dual antenna system combined with Gaussian process and Particle filter algorithms to achieve millimeter level localization accuracy. The system is capable of achieving millimeter level accuracy over 50m of length without an apparent estimation drift. The results were validated through experiments conducted using an extracted water pipe section.**

***Index Terms*— Automation Technologies for Smart Cities; Robotics and Automation in Construction; Robotics in Hazardous Fields; Field Robotics; Infrastructure Robotics; Localization;**

I. Introduction

PIPELINES transporting drinking water from treatment facilities or wells to customer's taps are found in millions of kilometers of length throughout the world. Overtime, the pipes can degrade due to a combination of factors such as pipe material, size, age, water quality, surrounding soil conditions and pressure zones [1]. Regular inspections are proven to be effective in early detection and intervention [2]. Majority of the water mains are small in size (less than 600mm diameter), where human entry is not possible, and for larger pipes, entering them is a health and safety risk. Therefore, water utilities use a variety of robotic technologies [3]–[8] to detect degraded regions. Once discovered, expensive pipe replacements are generally carried out (in Australia, it ranges from $400/m for small pipes to $4000/m for large pipes [9]). Application of lining technologies as a cost effective renewal method is often utilized. However, they themselves require monitoring over long periods of time for deterioration. Monitoring defect evolution requires an accurate in-pipe localization method, which is addressed in this paper due to the requirement of defect correspondence in multiple deployments and estimating accurate longitudinal defect sizing.

In-pipe robot localization through wheel odometry is inaccurate due to wheel slips associated with water puddles and build ups, and inherent drifts [2]. Dead reckoning techniques based on inertial measurement units (IMUs) that employ magnetometers have limitations due to surrounding metallic structures, and use of accelerometers/gyroscopes is challenging due to lack of agility, inherent drifts and sensor biases [10]. The length of the deployed tether is commonly used for in-pipe robot localization as reported in [11] while [12] attempts to integrate IMU data with tether cable encoder data for in-pipe localization. These technologies can provide approximate robot localization, which can be reasonable for many applications. However, they fail to achieve the accuracy required for the application focused in this paper. The GPS does not work in in-pipe environments due to lack of visibility of satellites. Use of visual odometry techniques utilizing stereo cameras [13], monocular cameras [14], RGB-D sensors combined with machine learning algorithms [15] and monocular fish-eye cameras [16] for in-pipe robot localization have also been reported in the literature. However, in the context of liner applied pipes, there are very limited discernible features. Further, the application of liners alters the visual features. Ultrasound sensor based localizers [17] reported limited applications in metallic pipes.

Therefore, researchers are exploring alternative sensing modalities such as UHF-RFID, which has further advantages of measuring temperature and humidity conditions [18]–[21]. The technology is targeted at new or newly renewed pipes. Even large water utilities such as Sydney Water Corporation's annual renewal length is limited to a 2km distance. Tag installation can be selectively done, for example in crucial and difficult to access areas (middle of a city). Therefore, it is feasible to install UHF-RFID tags (as part of the liners or as tags embedded in new pipes) in identified crucial assets to monitor performance. Generally, renewed assets can last for 20 years and these tags are expected to last longer. The pipe infrastructure deterioration rate is very slow and hence inspections are generally less frequent.

RFID localization has been explored by many researchers in achieving indoor localization [22]–[26] and outdoor localization [27]–[30] with promising accuracy. However, these methods are not readily transferable into metallic pipes as they have unique challenges due to RFID signal behaviors [9], [31] causing multiple signal peaks.

In our previous work, we reported the use of a single UHF-

Manuscript received: November 18, 2021; Revised February 9, 2022; Accepted March 28, 2022.

This paper was recommended for publication by Editor Javier Civera upon evaluation of the Associate Editor and Reviewers' comments. This work was supported by the University of Technology Sydney (UTS) through the Faculty of Engineering and Information Technology (FEIT) Tech Lab Blue Sky Research Grant.

All the authors are with the iPipes Lab, UTS Robotics Institute, Faculty of Engineering and Information Technology, University of Technology Sydney, Sydney, New South Wales, 2007, Australia (e-mail: Amal.Gunatilake@uts.edu.au; Sarath.Kodagoda@uts.edu.au; Karthick.Thiyagarajan@uts.edu.au).

Digital Object Identifier (DOI): see top of this page.

RFID antenna coupled with a Gaussian Process combined with a particle filter approach to achieve up to 15cm of accuracy [9]. However, the defect evolution monitoring requires a millimeter level of accuracy, and hence, the need for our further research work. Use of RFID dual antenna systems to improve localization accuracy for indoor and outdoor applications has been previously reported [24], [29], [30]. Therefore, in this letter, an attempt was made to achieve better localization accuracy by integrating a dual antenna system with a Gaussian Process and Particle filter based algorithm with an improved measurement model and improved signal processing. Further, the letter illustrates in-depth technical attributes of our work with extended experiments carried out to validate the results. The main contributions reported in this letter are:

1) Firstly, in-pipe localization problem was formulated as a particle filter combined with a Gaussian process (GP) using the UHF-RFID dual antenna system.
2) Secondly, use of a dual antenna system with both RSSI and phase data improved localization to millimeter level accuracy when compared with that of a single antenna system which had centimeter level accuracy.
3) Thirdly, experiments carried out on an extracted buried water pipe with a robot integrated dual UHF-RFID antenna system show the effectiveness of the proposed localization technology.

The remainder of this letter is structured as follows: Section II presents the development of an in-pipe robot system. Section III formulates the problem. In Section IV, we present the experimental results, while in Section V, we summarize the key outcomes and future work.

II. In-Pipe Robot System Development

Robotic development can be explained through the hardware and system architecture as shown in Fig. 1.

A. Hardware

Dual UHF-RFID antennas were mounted on the robot as shown in Fig. 1a. Both receivers were 915MHz general purpose panel RF antennas in the 902MHz to 928MHz range with 5.5dBi gains. An industry standard infrared laser distance sensor with 80m range at 1mm accuracy has been used as the localization ground truth. For comparison purposes, a standard wheel encoder with 2400 pulses per revolution has been used. Jetson Nano Developer kit board with Quad-core ARM 1.43 GHz CPU, 4 GB 64-bit LPDDR4 RAM was used as the central processing unit. The robotic crawler shown in Fig. 1a is 200mm wide, and 300mm tall with a height extendable platform, which can be deployed in most underground water pipelines above 0.3m in diameter. Based on our previous research work [9], "Tag A" type UHF-RFID tags were used and deployed inside the side surface of the pipe aligned longitudinally to the pipe axis as shown in Fig. 2.

B. Software

We utilized the Robotic Operating System (ROS) framework, with individual components being implemented as ROS nodes. Figure 1b describes the nodes and their interactions with reference to multi-hardware and software systems.

III. Particle Filter Based In-Pipe Robot Localization

Use of particle filters for UHF-RFID based localization is not uncommon due to its capability of handling complex observation models [29], [32]–[35]. Particle filter can also be combined with Gaussian process to improve non-liner modeling process [36], [37]. Let x_t be the robot's location at time t and z_t related to both RSSI and phase signal measurements received at time t. The process and observation models can be defined as follows:

$$x_t = g(x_{t-1}, \omega_t) \tag{1}$$

$$z_t = h(x_t, v_t) \tag{2}$$

where g and h are known functions. Recursive form with sequential estimates of distribution states at time $t-1$ can be expressed as below.

$$p(x_t|z_{1:t}) \propto p(z_t|x_t) \int p(x_t|x_{t-1}) p(x_{t-1}|z_{1:t-1}) dx_{t-1} \tag{3}$$

where, $p(x_t|x_{t-1})$ and $p(z_t|x_t)$ are probability distributions, and $\omega_t \in R^{d_u}$ and $v_t \in R^{d_v}$ denote white-noise independent of each other. To filter the sequential estimates of distribution at time $t-1$, N number of particles are generated and distributed along the pipe section in the form of $X_{t-1} = \left\{x_{t-1}^{(n)} | w_{t-1}^{(n)}\right\}_{n=1}^{N}$, where $w_{t-1}^{(n)}$ are the weights generated for the particles. The distribution can be approximated as in (4).

$$p(x_{t-1}|z_{1:t-1}) \approx \sum_{n=1}^{N} w_{t-1}^{(n)} \delta\left(x_{t-1} - x_{t-1}^{(n)}\right) \tag{4}$$

where $\delta()$ is the Dirac delta function. Therefore, (3) can be written as follows.

$$p(x_t|z_{1:t}) \propto p(z_t|x_t) \sum_{n=1}^{N} w_{t-1}^{(n)}\ p\left(x_t|x_{t-1}^{(n)}\right) \tag{5}$$

Phase data is noisier than RSSI data which is handled by introducing appropriate weights. For a given particle, assuming that the RSSI and phase data are uncorrelated, weight (w) is generated as,

$$w = mean\left(\left[\left|\begin{bmatrix} z_g^* \\ z_h^* \end{bmatrix} - \begin{bmatrix} z_g \\ z_h \end{bmatrix}\right| + \begin{bmatrix} \xi \\ 0 \end{bmatrix}\right] \times \begin{bmatrix} c & 0 \\ 0 & (1-c) \end{bmatrix}\right) \tag{6}$$

where z_g is the predicted RSSI measurement from the GP model formulation in Section III-B that maps to the particle; z_h is the raw phase signal measurement from the model that maps to the particle; z_g^* and z_h^* are the RSSI and phase measurements received from the robot at a particular time; ξ is the uncertainty that is derived from the GP; and c is a

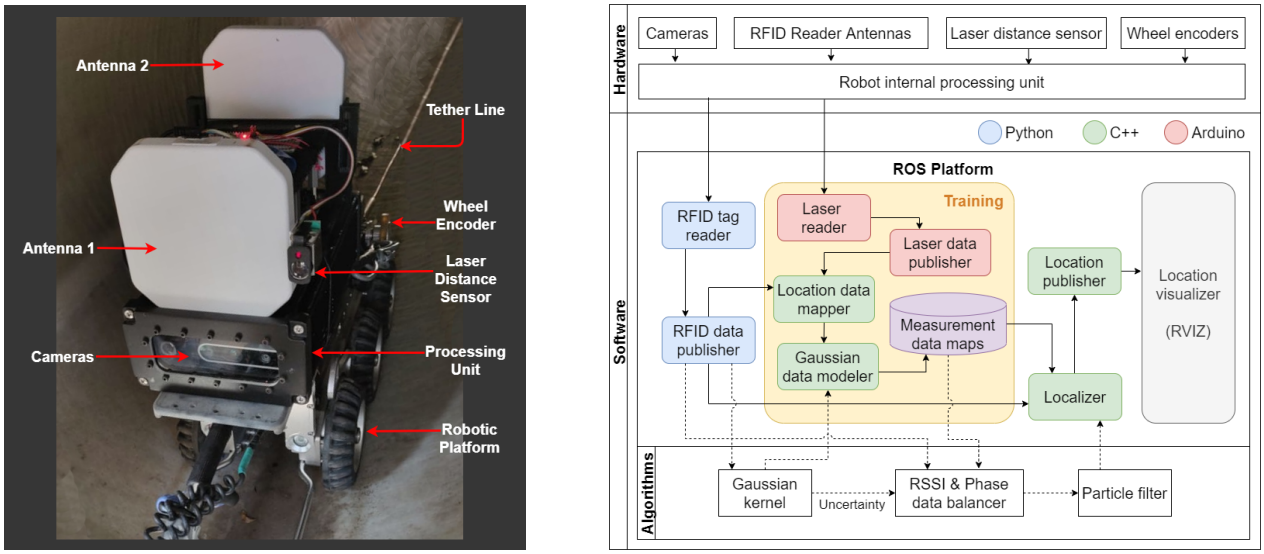

(a) (b)

Fig. 1: In-pipe robot system. (a) Robot integrated with two UHF-RFID reader antennas, and (b) System architecture.

normalization parameter capturing the different noise levels of RSSI and phase values.

The GP models are learned for each UHF-RFID tag from each antenna, the resulting predictions can lean towards over-confident estimates. To prevent such a phenomenon, the likelihood model is smoothed using (7):

$$p(z_{t[1:n]}|x_t) = \left(\prod_{i=1}^{n} p(z_{t[i]}|x_t)\right)^{\gamma} \tag{7}$$

where γ *is* the smoothing coefficient lies between 0 and 1.

A. Particle Re-sampling

Let $S_{t-1} = \left\{\left\{x_{t-1}^{(n)}, w_{t-1}^{(n)}\right\}, z_t\right\}$ be the state at $(t-1)$ that contains a set of particles and weights. z_t are the measurements sensed by the robot at time t. The following procedure is iteratively executed for $i = 1, 2, ...n$, where $S_t = \emptyset$ is the new set and γ is the normalization factor for weights:

- Sample index $\hat{i}$ from discrete distribution given by w_{t-1}.
- Sample x_t^i from $p(x_t|x_{t-1})$ using $x_{t-1}^{\hat{i}}$
- Reweight $w_t^i = p\left(z_t|x_t^i\right)$
- Update factor $\gamma = \gamma + w_t^i$
- Update new states $S_t = S_t \cup \left\{x_t^i, w_t^i\right\}$
- Normalise weights $w_t^i = \dfrac{w_t^i}{\gamma}$ for $i = 1, 2, ...n$

The steps in the particles have been calculated based on the robot's travel speed given by the central controlling system (based on the tether encoder).

B. Gaussian Process Based Measurement Model

Function–space view modeling was used to derive the GP, as described in [38]. Let $S = \{(x_1, y_1), (x_2, y_2), ..., (x_i, y_i), ..., (x_n, y_n)\}$ be the set of noisy RSSI training data samples, where x_i is the robot position and y_i is the corresponding RSSI value received by the robot. The prediction model relating to the robot's location and the RSSI measurement can be learned in the form of a function f as in (8):

$$y_i = f(x_i) + \epsilon \tag{8}$$

where ϵ is the zero mean Gaussian noise with a known σ_n^2 variance. Since the robot is moving along the axis of the pipeline, all input values x_i and target y_i values can be aggregated into vectors $\mathbf{x}$ and $\mathbf{y}$ respectively.

The GP enables correlation of the RSSI signal strength function values at different data points where the covariance of $f(x_p)$ and $f(x_q)$ values depends on the robot location input values of x_p and x_q. This relationship can be learned in the form of a kernel $k(x_p, x_q)$ to generate the training data model. The squared exponential kernel is selected to learn the non-linear regression problem, which is defined as,

$$k(x_p, x_q) = \sigma_f^2 \; exp\left\{-\frac{1}{2\beta^2}|x_p - x_q|^2\right\} \tag{9}$$

where β and σ_f^2 are hyper-parameters. Covariance of the GP is defined as,

$$cov(y_p, y_q) = k(x_p, x_q) + \sigma_n^2 \delta_{pq} \tag{10}$$

where δ_{pq} is either one or zero depending on $p = q$, and σ_n^2 is the observation noise. For all robot locations, $\mathbf{x}$ corresponding co-variance function of the observations $\mathbf{y}$ can be defined as,

$$cov(\mathbf{y}) = \mathbf{K} + \sigma_n^2 I \tag{11}$$

$$\mathbf{K}[p, q] = k(x_p, x_q) \tag{12}$$

where $\mathbf{K}$ is the covariance matrix for all data inputs $\mathbf{x}$.

Let x_* be an arbitrary robot location, where the RSSI signal strength needs to be estimated based on the function

value $f(x_*)$ from training data $\mathbf{x}$ and $\mathbf{y}$. The posterior distribution μ_{x_*} and the associated uncertainty $\sigma^2_{x_*}$ can be calculated as in (13) and (14):

$$\mu_{x_*} = \mathbf{k}_*^T \left(K + \sigma_n^2 I\right)^{-1} \mathbf{y} \tag{13}$$

$$\sigma^2_{x_*} = k(x_*, x_*) - \mathbf{k}_*^T \left(K + \sigma_n^2 I\right)^{-1} \mathbf{k}_* \tag{14}$$

where $\mathbf{k}_*$ is a covariance vector from the matrix $\mathbf{K}$ for corresponding input values. Further, hyper-parameters are estimated by minimizing negative log marginal likelihood,

$$\log\ p(\mathbf{y}|\mathbf{x}, \theta) = -\frac{1}{2}\mathbf{y}^T \left(K + \sigma_n^2 I\right)^{-1} \mathbf{y} - \frac{1}{2}\ \log\ |K + \sigma_n^2 I| - \frac{1}{2}\ \log\ 2\pi \tag{15}$$

where $\theta = \left\{\sigma_n^2, \beta, \sigma_f^2\right\}$.

IV. Experiments & Results

This section presents a discussion on data collection, analysis and performance.

A. In-pipe Robotic Data Collection and Processing

The use of tethered heavy crawler robots in pipelines with curves and bends is discouraged since the tether tends to tangle or rip. In fact, most water pipe inspections of medium-sized pipe (diameters of 300mm to 900mm) inspections are carried out over shorter lengths (less than 500m) and are relatively straight. Manhole to manhole deployments are common in medium-sized (900mm - 1500mm diameter) non-traversable sewage lines ranging from $100 - 300$ meters and they are mostly straight pipe sections that simplified the localisation problem. However, this technique may be updated using an IMU sensor and/or prior knowledge of network designs to deal with changes in orientation in pipe settings with probable bends.

The robot equipped with dual UHF-RFID antennas (Fig. 2) was deployed in 5m long, 0.6m diameter cast iron cement lined water pipe extracted from the Sydney Water pipe network. The robot was deployed 10 times inside the 5m pipe, and in each deployment we attached new UHF-RFID tags (in total of 50 different tags were used) that mimic approximately a 50-meter-long RFID pipe scan. It is an approximation that we used due to the COVID restrictions preventing us from using a longer pipe section to carry out the experiments. The laser distance measurement unit provided an accurate location of the robot (ground truth).

Learning a general GP model based on a single RIFD was not successful due to significant variability of the intra-tag data. Learning a general GP sensor model using all the UHF-RFID tags was also inaccurate due to various concatenated errors. Figure 5 shows the distance aligned RFID data which seems scattered without showing a significant pattern making it nontrivial to learn a model. This can be due to several reasons including the effects of tag placements and the pipe environment. In the current research, each RSSI signal generated from different UHF-RFID tags from the different antennas (Fig. 3) was trained with a separate GP model. Figure 4 shows part of the training data of one antenna with six tags.

Fig. 2: Robot inside a pipe.

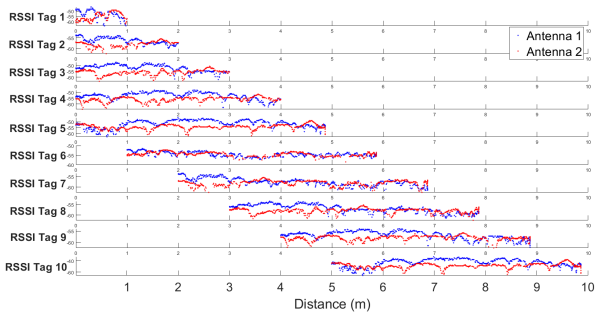

Fig. 3: Training data sample.

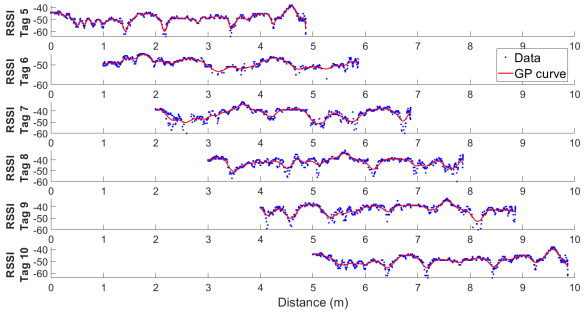

Fig. 4: Gaussian kernel training for each UHF-RFID tag signal.

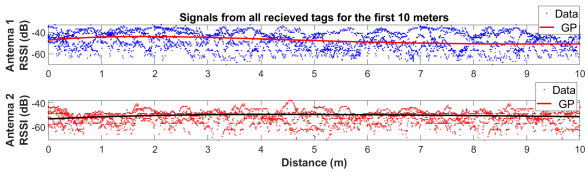

Fig. 5: Single Gaussian kernel training for all received UHF-RFID tags.

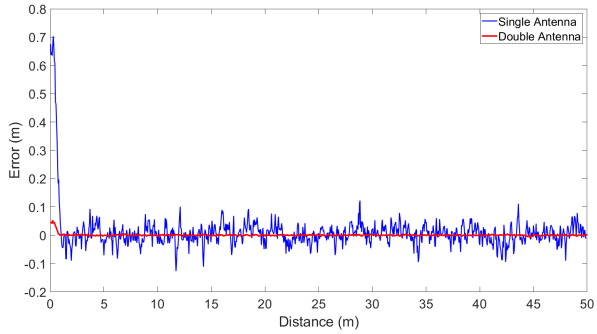

Fig. 6: Single antenna performance vs double antenna performance comparison.

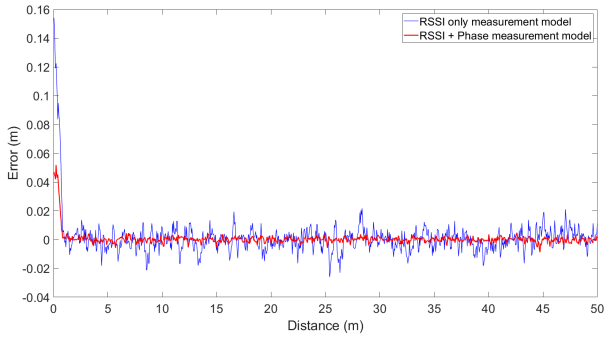

Fig. 7: RSSI and Phase data measurement model performance evaluation.

B. Number of antennas and signals

In this section, we investigated the effects of introducing the dual antenna system. We found that the addition of the dual antenna system contributes to a 20-fold location accuracy improvement when compared with a single antenna system, as shown in Fig. 6. Incorporation of phase data with RSSI data contributes to 10-fold improvement of the robot localization accuracy when comparing with RSSI data alone as shown in Fig. 7.

C. RFID tag distribution

In this section, we present the robot localization errors associated with tag distribution as sparsity is preferred due to economical reasons. As shown in Fig. 8, the smaller the inter tag distance, higher the localization accuracy. Inter tag distance of 1m resulted in millimeter level localization accuracy. Spacing of 2m, 3m gives rise to larger errors (0.016m and 0.049m mean errors respectively). Therefore, the utilities can choose the tag distribution based on the accuracy requirements.

D. Number of particles and their distribution

In general, an increase in the number of particles contributes to better localization accuracy, however, with an increased computational burden (see Fig. 9). With the available limited on-board computing capability, it was decided

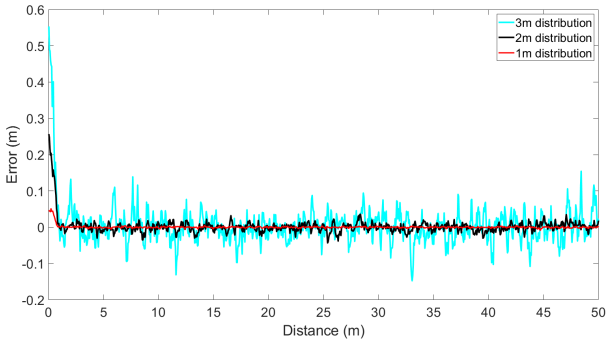

Fig. 8: Tag distribution performance comparison.

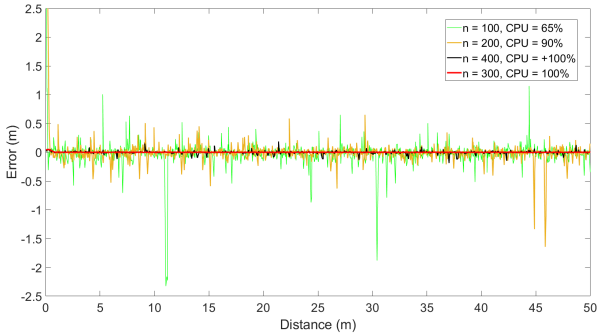

Fig. 9: Number of particles performance comparison.

that 300 particles as a reasonable compromise between the localization accuracy and computational time.

Fig. 10 shows different particle distributions and related performances. Spreading the particles within the whole pipe section delayed the convergence. Therefore, knowing the approximate start location, the particles were distributed locally to improve the convergence speed.

E. Performance Comparison with other Localization Methods

Using all the above discussed improvements, a final mean localization accuracy of 0.0018m was achieved with 0.0016 standard deviation. The Root Mean Square Error (RMSE) is shown in Fig. 11. Figure 12 shows the whiskers plot for 20 sets of trials performed with 0.06m of white Gaussian noise for the robot motion. The uncertainty variations along the

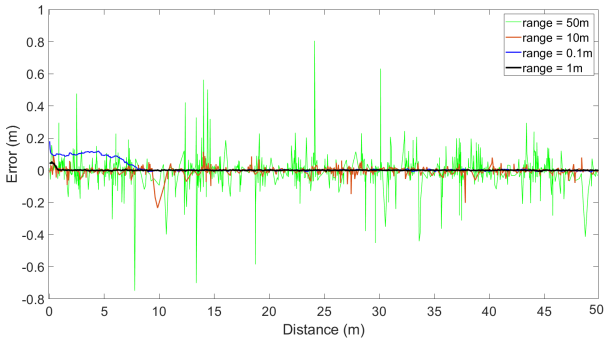

Fig. 10: Particle distribution performance comparison.

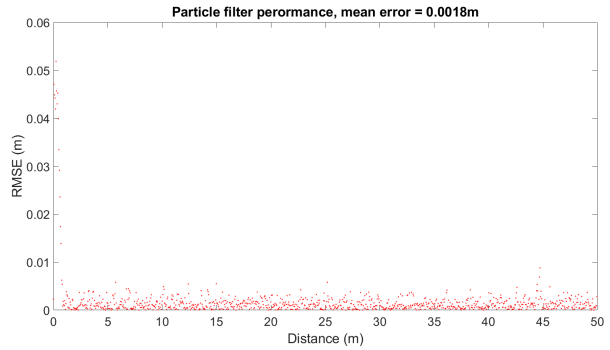

Fig. 11: Particle filter performance. Mean error: 0.0018m

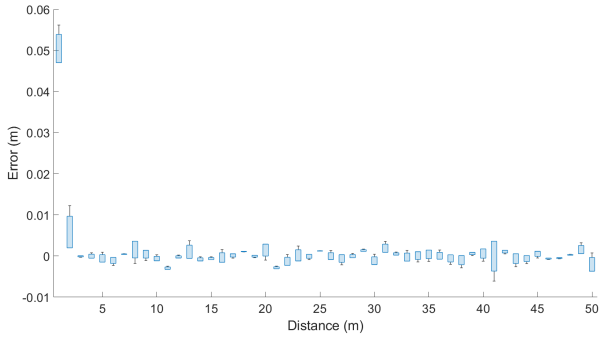

Fig. 12: Whisker plot of 20 sets of trials with 0.06m of white Gaussian noise for the robot motion.

pipe in general are attributed to the quality of the UHF-RFID tag, tag orientation, tag placement, pipe local conditions and robot's agile movement.

Table I shows the result comparisons of different localization methods for 50m travel distance. Although the accuracy of the encoder is reasonable for some water industry applications, error drifts significantly causing larger errors in longer deployments. The nearest UHF-RFID tag localization method used for outdoor and indoor localization produces approximately 3m of mean error due to signal reflections inside the metallic pipe. On the contrary, the proposed UHF-RFID localization methods produce higher accuracy and consistency along the pipe for longer distances, making them very effective for the application.

Localization method	Error RMSE (m)	Error Std dev (m)	Error Max (m)
Encoder (error accumulates with distance)	0.404	0.413	0.817
Nearest tag localization without GP or PF	3.165	2.045	5.21
Single antenna localization	0.015	0.007	0.022
Dual antenna RSSI signal only	0.006	0.012	0.02
Dual antenna RSSI + Phase localization	0.0018	0.0005	0.0023

TABLE I: Localization methods performance comparisons for 50m of pipe length.

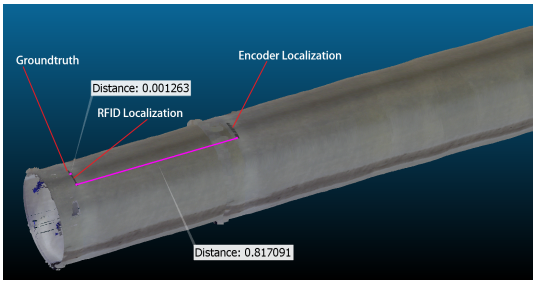

Fig. 13: Laser profile localization tests - RFID vs Encoder.

Figure 13 shows the end of the 50m long run, 3D laser profile alignments with the ground truth, encoder, and UHF-RFID localization. As seen in the image, a mark on the pipe crown was used to measure localization misalignment. It can be seen that the encoder-odometry-based laser profile is 0.817m behind the ground truth laser profile. The UHF-RFID-localized laser profile has been perfectly aligned with the ground truth laser profile, giving 1mm of accuracy. This demonstrates the effectiveness of the proposed localization approach for accurately aligning defects in laser profiles to monitor their evolution.

V. Conclusion & Future Work

In this letter, we presented the development of a robotic system that uses UHF-RFID signals to localize itself inside underground pipeline infrastructure. The system is equipped with two antennas and uses a Gaussian process combined particle filter algorithm for accurate robot localization. The accuracy of the robot localization has been further enhanced by integrating RSSI and Phase shift data together in the particle filter measurement model. The system was validated in Sydney Water's extracted drinking water pipe. The results show that the proposed system is capable of localizing the robot inside a pipeline with millimeter level accuracy, significantly outperforming other methods. Finally, the solution was evaluated using the reconstructed pipe laser profile data showing the effectiveness of the methodology. In future, we plan to address the inherent behavior of tags once embedded in cement near metallic surfaces [39] and related localization effects. Further, we plan to conduct experiments in longer pipe sections in different pipe environments to study the RFID tag signal repeatability behaviors and possibility of developing a generalized GP model for improving the deployment effectiveness.

References

[1] Z. Liu and Y. Kleiner, "State of the art review of inspection technologies for condition assessment of water pipes," *Measurement*, vol. 46, no. 1, pp. 1–15, Jan. 2013.

[2] C. Rizzo, T. Seco, J. Espelosín, F. Lera, and J. L. Villarroel, "An alternative approach for robot localization inside pipes using RF spatial fadings," *Robotics and Autonomous Systems*, vol. 136, p. 103702, 2021.

[3] J. V. Miro, D. Hunt, N. Ulapane, and M. Behrens, "Towards automatic robotic NDT dense mapping for pipeline integrity inspection," in *Field and Service Robotics*. Springer International Publishing, Nov. 2017, pp. 319–333.

[4] J. M. M. Tur and W. Garthwaite, "Robotic devices for water main in-pipe inspection: A survey," *Journal of Field Robotics*, vol. 27, no. 4, pp. 491–508, Jun. 2010.

[5] J. V. Miro, N. Ulapane, L. Shi, D. Hunt, and M. Behrens, "Robotic pipeline wall thickness evaluation for dense nondestructive testing inspection," *Journal of Field Robotics*, vol. 35, no. 8, pp. 1293–1310, Nov. 2018.

[6] A. Gunatilake, L. Piyathilaka, S. Kodagoda, S. Barclay, and D. Vitanage, "Real-Time 3D Profiling with RGB-D Mapping in Pipelines Using Stereo Camera Vision and Structured IR Laser Ring," in *2019 14th IEEE Conference on Industrial Electronics and Applications (ICIEA)*, 2019, pp. 916–921.

[7] A. Gunatilake, L. Piyathilaka, A. Tran, V. K. Vishwanathan, K. Thiyagarajan, and S. Kodagoda, "Stereo Vision Combined With Laser Profiling for Mapping of Pipeline Internal Defects," *IEEE Sensors Journal*, vol. 21, no. 10, pp. 11 926–11 934, 2021.

[8] N. Ulapane, K. Thiyagarajan, J. V. Miro, and S. Kodagoda, "Surface representation of pulsed eddy current sensor signals for improved ferromagnetic material thickness quantification," *IEEE Sensors Journal*, vol. 21, no. 4, pp. 5413–5422, Feb. 2021.

[9] A. Gunatilake, M. Galea, K. Thiyagarajan, S. Kodagoda, L. Piyathilaka, and P. Darji, "Using UHF-RFID Signals for Robot Localization Inside Pipelines," in *2021 IEEE 16th Conference on Industrial Electronics and Applications (ICIEA)*, 2021, pp. 1109–1114.

[10] R. Worley, K. Ma, G. Sailor, M. M. Schirru, R. Dwyer-Joyce, J. Boxall, T. Dodd, R. Collins, and S. Anderson, "Robot localization in water pipes using acoustic signals and pose graph optimization," *Sensors*, vol. 20, no. 19, p. 5584, Sep. 2020.

[11] H. Lim, J. Y. Choi, Y. S. Kwon, E.-J. Jung, and B.-J. Yi, "SLAM in indoor pipelines with 15mm diameter," in *2008 IEEE International Conference on Robotics and Automation*. IEEE, 2008, pp. 4005–4011.

[12] A. C. Murtra and J. M. M. Tur, "IMU and cable encoder data fusion for in-pipe mobile robot localization," in *2013 IEEE Conference on Technologies for Practical Robot Applications*. IEEE, 2013, pp. 1–6.

[13] P. Hansen, H. Alismail, B. Browning, and P. Rander, "Stereo visual odometry for pipe mapping," in *2011 IEEE/RSJ International Conference on Intelligent Robots and Systems*. IEEE, 2011, pp. 4020–4025.

[14] P. Hansen, H. Alismail, P. Rander, and B. Browning, "Monocular visual odometry for robot localization in LNG pipes," in *2011 IEEE International Conference on Robotics and Automation*. IEEE, 2011, pp. 3111–3116,.

[15] D. Alejo, F. Caballero, and L. Merino, "RGBD-based robot localization in sewer networks," in *2017 IEEE/RSJ International Conference on Intelligent Robots and Systems*. IEEE, 2017, pp. 4070–4076.

[16] P. Hansen, H. Alismail, P. Rander, and B. Browning, "Visual mapping for natural gas pipe inspection," *The International Journal of Robotics Research*, vol. 34, no. 4-5, pp. 532–558, Nov. 2014.

[17] K. Ma, J. Zhu, T. J. Dodd, R. Collins, and S. R. Anderson, "Robot mapping and localisation for feature sparse water pipes using voids as landmarks," in *Towards Autonomous Robotic Systems*. Springer International Publishing, 2015, pp. 161–166.

[18] X. Wang, J. Zhang, Z. Yu, S. Mao, S. C. G. Periaswamy, and J. Patton, "On remote temperature sensing using commercial UHF RFID tags," *IEEE Internet of Things Journal*, vol. 6, pp. 10 715–10 727, 2019.

[19] J. Virtanen, L. Ukkonen, T. Björninen, L. Sydänheimo, and A. Z. Elsherbeni, "Temperature sensor tag for passive uhf rfid systems," in *2011 IEEE Sensors Applications Symposium*, 2011, pp. 312–317.

[20] E. M. Amin, M. S. Bhuiyan, N. C. Karmakar, and B. Winther-Jensen, "Development of a low cost printable chipless rfid humidity sensor," *IEEE Sensors Journal*, vol. 14, no. 1, pp. 140–149, 2014.

[21] I. Gammoudi, B. Aissa, M. Nedil, and M. M. Abdallah, "Cnt-rfid passive tag antenna for gas sensing in underground mine," in *2015 IEEE International Symposium on Antennas and Propagation USNC/URSI National Radio Science Meeting*, 2015, pp. 1758–1759.

[22] F. Bernardini, A. Buffi, D. Fontanelli, D. Macii, V. Magnago, M. Marracci, A. Motroni, P. Nepa, and B. Tellini, "Robot-based indoor positioning of uhf-rfid tags: The sar method with multiple trajectories," *IEEE Transactions on Instrumentation and Measurement*, vol. 70, pp. 1–15, 2021.

[23] E. DiGiampaolo and F. Martinelli, "A robotic system for localization of passive uhf-rfid tagged objects on shelves," *IEEE Sensors Journal*, vol. 18, no. 20, pp. 8558–8568, 2018.

[24] J. Zhang, Y. Lyu, J. Patton, S. C. G. Periaswamy, and T. Roppel, "BFVP: A Probabilistic UHF RFID Tag Localization Algorithm Using Bayesian Filter and a Variable Power RFID Model," *IEEE Transactions on Industrial Electronics*, vol. 65, no. 10, pp. 8250–8259, 2018.

[25] S. R. Rusu, M. J. D. Hayes, and J. A. Marshall, "Localization in large-scale underground environments with rfid," in *2011 24th Canadian Conference on Electrical and Computer Engineering(CCECE)*, 2011, pp. 001 140–001 143.

[26] A. Motroni, P. Nepa, A. Buffi, and B. Tellini, "Robot localization via passive uhf-rfid technology: State-of-the-art and challenges," in *2020 IEEE International Conference on RFID (RFID)*, 2020, pp. 1–8.

[27] A. Buffi, P. Nepa, and R. Cioni, "Sarfid on drone: Drone-based uhf-rfid tag localization," in *2017 IEEE International Conference on RFID Technology Application (RFID-TA)*, 2017, pp. 40–44.

[28] A. Motroni, P. Nepa, A. Buffi, and B. Tellini, "A phase-based method for mobile node localization through uhf-rfid passive tags," in *2019 IEEE International Conference on RFID Technology and Applications (RFID-TA)*, 2019, pp. 470–475.

[29] C. Li, L. Mo, and D. Zhang, "Review on uhf rfid localization methods," *IEEE Journal of Radio Frequency Identification*, vol. 3, no. 4, pp. 205–215, 2019.

[30] C. C. Cruz, J. R. Costa, and C. A. Fernandes, "Hybrid uhf/uwb antenna for passive indoor identification and localization systems," *IEEE Transactions on Antennas and Propagation*, vol. 61, no. 1, pp. 354–361, 2013.

[31] A. Gunatilake, K. Thiyagarajan, and S. Kodagoda, "Evaluation of Battery-free UHF-RFID Sensor Wireless Signals for In-pipe Robotic Applications," in *2021 IEEE SENSORS*, 2021, pp. 1–4.

[32] P. Sarkar, "Sequential monte carlo methods in practice," *Technometrics*, vol. 45, no. 1, p. 106, 2003.

[33] M. Vemula, M. F. Bugallo, and P. M. Djuric, "Performance comparison of gaussian-based filters using information measures," *IEEE Signal Processing Letters*, vol. 14, no. 12, pp. 1020–1023, 2007.

[34] L. Li, Z. Yi, and W. Xie, "Gaussian sum quadrature particle filtering," in *2014 12th International Conference on Signal Processing (ICSP)*, 2014, pp. 234–238.

[35] J. Xian and Y. Geng, "Multi-user detection based on gaussian particle filter in impulsive noise," in *2013 2nd International Symposium on Instrumentation and Measurement, Sensor Network and Automation (IMSNA)*, 2013, pp. 349–352.

[36] Y. Xu, K. Xu, J. Wan, Z. Xiong, and Y. Li, "Research on particle filter tracking method based on kalman filter," in *2018 2nd IEEE Advanced Information Management,Communicates,Electronic and Automation Control Conference (IMCEC)*, 2018, pp. 1564–1568.

[37] N. Y. Ko and T. G. Kim, "Comparison of kalman filter and particle filter used for localization of an underwater vehicle," in *2012 9th International Conference on Ubiquitous Robots and Ambient Intelligence*, 2012, pp. 350–352.

[38] C. E. Rasmussen, *Gaussian Processes in Machine Learning*. Berlin, Heidelberg: Springer Berlin Heidelberg, 2004, pp. 63–71.

[39] A. Michel, P. Nepa, and M. R. Pino, "On rfid tag detection inside metal pipes," in *2018 IEEE International Symposium on Antennas and Propagation USNC/URSI National Radio Science Meeting*, 2018, pp. 681–682.